Morphological and Conformational Changes of Poly(trimethylene terephthalate) during Isothermal Melt Crystallization

Nadarajah Vasanthan,* Sabahattin Ozkaya, and Mustafa Yaman†

Department of Chemistry, Long Island University, One University Plaza, Brooklyn, New York 11201

Received: June 24, 2010; Revised Manuscript Received: September 8, 2010

The isothermal melt crystallization of poly(trimethylene terephthalate) (PTT) has been investigated using differential scanning calorimetry (DSC), optical microscopy, and Fourier transform infrared (FTIR) spectroscopy. Triple-melting endotherms were dominant at crystallization temperatures (T_c) below 195 °C, while double-melting endotherms were dominant at T_c above 195 °C. These multiple-melting behaviors were attributed to melting and recrystallization as well as thermal stability of the crystallites. The difference in crystallinity observed between melt-crystallized PTT films before and after cooling to room temperature was attributed to lamellar thickening. The kinetics of isothermal melt crystallization of PTT was analyzed using an Avrami equation, and the rate constant (k) and $t_{1/2}$ increased with increasing T_c. An Avrami exponent $n = 2-3$ was obtained for the PTT melt crystallized from 150 to 205 °C, suggesting two-dimensional to three-dimensional growth with heterogeneous nucleation and was confirmed by polarized optical microscopy. The bands at 1358 and 976 cm^{-1} associated with gauche and trans conformations of $-OCH_2CH_2CH_2O-$ were used to determine gauche and trans conformations assuming a two-phase conformational model. The crystalline and the amorphous gauche conformations were separated by combining them with DSC crystallinity. It was shown that the crystalline gauche conformation increased at the expense of the amorphous trans conformation. No significant change in the amorphous gauche conformation was found. On the other hand, the crystalline and amorphous gauche conformations were found to increase with the annealing temperature (T_a) at the expense of the trans conformations during the annealing of PTT. The difference between melt crystallization and annealing was also discussed.

Introduction

Poly(trimethylene terephthalate) (PTT) is a semicrystalline aromatic polyester with three methylene units in its monomer units and is a promising material for engineering applications such as films and fibers. PTT has not been studied in detail compared with other polyesters such as poly(ethylene terephthalate) (PET) and poly(butylene terephthalate) (PBT) because PTT was not readily available until recently.[1−10] PTT has been introduced commercially by Shell Chemicals under the trade name of Corterra. PTT exhibits a notably higher elastic recovery (>90%) and a lower modulus than both PET and PBT, and the elastic recovery of PTT is comparable to or better than the elastic recovery of nylon 6 and nylon 66.[1] Therefore, it was assumed that PTT has many advantages over these nylons and other aromatic polyesters. These properties are very desirable for carpet and textile applications. It has also been shown that PTT can be used in the field of optical communications, optical data processing, and nonlinear optics because of its high birefringence and luminous transmittance.[6]

Thermal properties such as the glass transition (T_g), crystallization, and the melting behavior of PTT have been previously reported.[11−15] The isothermal and nonisothermal crystallization and the crystallization kinetics of PTT have been studied by a number of groups. The crystallization kinetics of PET, PTT, and PBT were compared in some of the earlier studies and showed that the number of methylene groups in the glycol unit dictates the crystallization behavior of aromatic polyesters. PET crystallizes very slowly, and PBT crystallizes relatively fast, but PTT has an intermediate crystallization rate compared to PET and PBT.[12] PTT can crystallize, and only one crystal form has been identified to date. The crystal structure of PTT has been examined.[16−18] The unit cell of this crystal form has been determined to be triclinic with $a = 4.637$ Å, $b = 6.226$ Å, $c = 18.64$ Å, $\alpha = 98.4°$, $\beta = 93°$, $\gamma = 111.5°$, and a density of 1.432 g/cm^3. A single chain passes through each unit cell, and two monomer units are present in a unit cell, forming a 2/1 helix. It has been revealed that the trimethylene glycol unit of PTT ($-OCH_2CH_2CH_2O-$) adopts a highly contracted trans−gauche−gauche−trans conformation that is more contracted than PBT's conformation.[19,20]

Vibrational spectroscopy has been used extensively to study the microstructure changes such as crystallinity, conformational changes, and crystalline and amorphous orientations of PET during thermally or strain-induced crystallization, and this spectroscopy has received significant attention from academic and industrial laboratories.[21−25] IR spectroscopy has been used to some extent to study the crystallization of PTT[26−30] and IR bands associated with trans and gauche conformations. Fourier transform infrared (FTIR) spectra have been used to monitor conformational changes during the annealing of PTT. We have recently developed a method to determine quantitatively the crystalline and amorphous gauche and the amorphous trans conformations of PTT.[29] To better understand the early stage of melt crystallization and annealing, conformational changes were followed using a combination of differential scanning calorimetry (DSC) and FTIR spectroscopy. It is shown that the mechanism associated with the early stage of crystallization is different for melt crystallization compared to annealing of PTT.

* Corresponding author.
† Current address: TÜBİTAK Marmara Research Centre, Food Institute, 41470, Gebze, Kocaeli, Turkey.

10.1021/jp1058484
Published on Web 09/29/2010

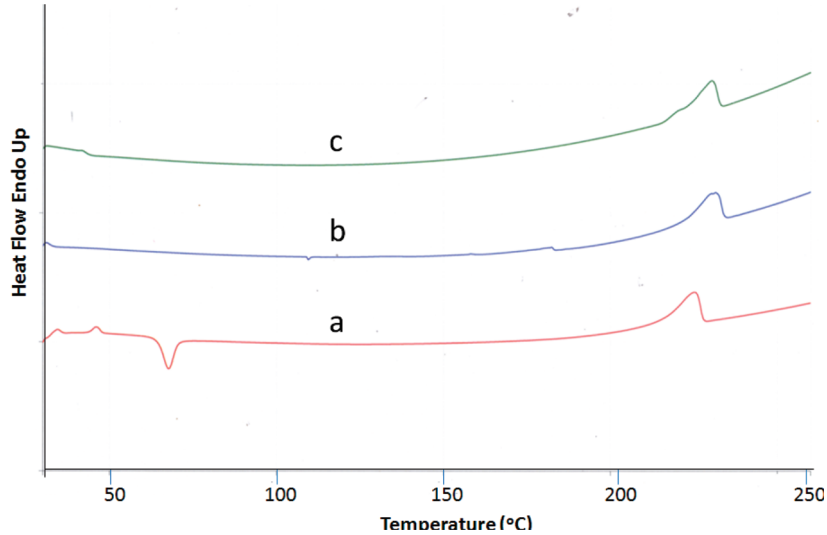

Figure 1. DSC heating scans of PTT films: amorphous (a), melt crystallized at 110 °C (b), and melt crystallized at 190 °C (c).

2. Experimental Section

2.1. Materials. PTT was supplied in pellet form with an intrinsic viscosity of 0.85 dL/g (determined in dichloroactetic acid) by the Shell Chemical Co. The molecular weight and the number average molecular weight of PTT resin were determined to be 35 200 and 17 300 g/mol. The molecular weight distribution was about 2.0. Approximately four to five PTT pellets dried under a vacuum were placed between Teflon sheets and melt pressed between two preheated platens in a Carver press at 260 °C under 10 000 lb of pressure. Films were removed after 5 min and subsequently quenched in an ice cold water bath to prevent further crystallization. Films obtained by this method were predominantly amorphous. These films were dried in a vacuum prior to crystallization studies.

2.2. Differential Scanning Calorimetry. DSC measurements were performed using a Perkin-Elmer DSC 7 between 30 and 260 °C in a dry nitrogen atmosphere and at a heating rate of 10 °C/min using 4−5 mg of sample. Calibration of the temperature and heat of fusion was carried out using indium and zinc standards. The crystallinity of melt-crystallized PTT was calculated by using the following equation:

$$X_c = (\Delta H_s - \Delta H_{cc})/\Delta H_o$$

where ΔH_s is the heat of fusion of the sample and ΔH_{cc} is the heat of the cold crystallization. ΔH_o was taken as 145.63 J/g.[13]

2.3. Melt Crystallization. Melt crystallization of the PTT films was carried out in the oven and inside the DSC apparatus by three different methods: (1) amorphous films were heated to 260 °C for 5 min and quickly transferred into the oven preset at the desired crystallization temperatures (T_c) from 110 to 205 °C, allowed to crystallize for 1 h at T_c, and quenched to room temperature; (2) amorphous PTT films were heated to 260 °C from 30 °C at a rate of 10 °C/min, held at 260 °C for 5 min, cooled to the desired T_c at a rate of 100 °C/min, allowed to crystallize for 1 h, and subsequently cooled to room temperature; (3) amorphous PTT films were heated to 260 °C from 30 °C at a rate of 10 °C/min, held at 260 °C for 5 min, cooled to the desired T_c at a rate of 100 °C/min, and allowed to crystallize for 1 h. All of the films were heated to 260 °C to determine the melting behavior of melt-crystallized PTT. Crystallization kinetics were performed by the following procedure. Amorphous PTT films were heated to 260 °C from 30 °C at a rate of 10 °C/min, held at 260 °C for 5 min, and cooled to the desired T_c at a rate of 100 °C/min. The crystallization exotherm was recorded as a function of time until the samples ceased to further crystallize.

2.4. FTIR Spectroscopy. FTIR spectroscopic measurements were made on a Nicolet Magna IR 760 spectrometer with a resolution of 4 cm^{-1}. At least 128 scans were coadded to achieve an adequate signal-to-noise ratio. Crystallization of PTT was followed by FTIR spectroscopy using a region of 600−4000 cm^{-1} in the spectra. Selected IR bands were resolved using a peak fitting program (Galactic) to determine the area under the peaks. The bands were assumed to be Lorentzian in shape with a linear baseline. Peak areas of the isolated infrared bands were measured directly by using the peak area tool of the Omnic software. At least three determinations were made, and the average values are reported. The error analysis was evaluated by using the standard deviation.

2.5. Optical Microscopy. Optical microscopic studies were performed using a Nikon polarizing optical microscope (PLM) equipped with a 35 mm Minolta X-700 camera. A double-focus X-40 and X-20 objective was used as the eyepiece. Photographs and measurements were made using the Spot Advanced program.

3. Results and Discussion

3.1. Melt Crystallization Behavior of PTT. The isothermal melt crystallization of PTT is carried out by three different methods, and the details of the methods of crystallization are given in the Experimental Section. The major difference between these methods is the rate of cooling after the melt crystallization. All PTT films crystallized inside the oven were quenched in the air quickly to room temperature, while after the melt crystallization of PTT inside the DSC apparatus, all PTT samples were slowly cooled to room temperature. Figure 1 shows the DSC heating scans of an amorphous PTT film and melt-crystallized PTT inside the oven at 110 and 190 °C. The DSC scan of amorphous PTT shows three transitions with a glass transition temperature (T_g) of 44 °C, melting temperature (T_m) of 228 °C, and cold crystallization temperature (T_{cc}) of 73 °C, which are very close to previously reported values. Substantial changes occur in the DSC scans of melt-crystallized PTT films as a function of the crystallization temperature T_c, shown in Figure 1. T_g and T_{cc} disappear completely in the DSC scans of melt-crystallized PTT at 110 and 190 °C. A similar observa-

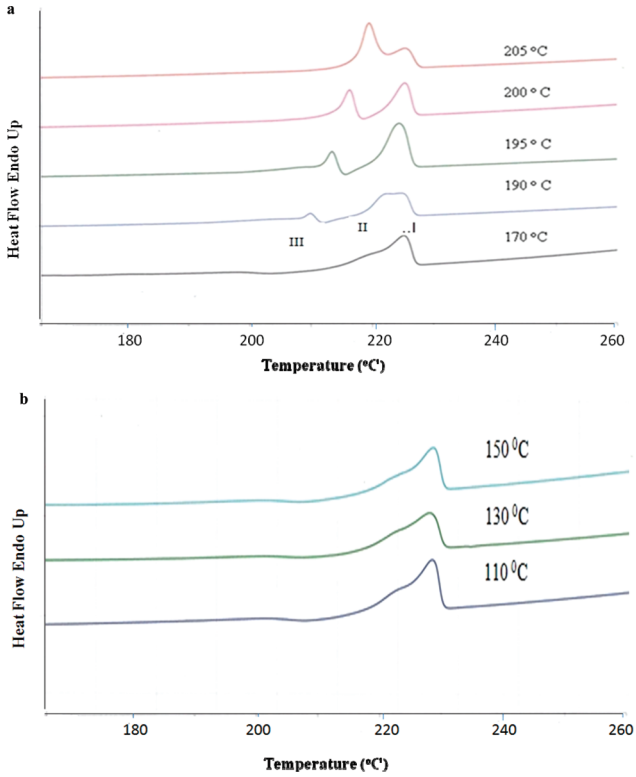

Figure 2. (a) DSC scans recorded at 10 °C/min for PTT films isothermally crystallized from the melt at different crystallization temperatures (170−205 °C) inside the DSC apparatus. (b) DSC scans recorded at 10 °C/min for PTT samples isothermally crystallized from the melt at different crystallization temperatures (110−150 °C) inside the DSC apparatus.

tion has been observed for annealed PTT previously, and the disappearance of T_{cc} was attributed to thermally induced crystallization.[28] The mobility of the polymer chain in the amorphous phase might be reduced during thermally induced crystallization, leading the T_{cc} to increase and disappear after a certain T_c. Drawing of PTT films has also been studied by DSC,[3] and it has been shown that the cold crystallization peak appears only below a draw ratio of 2.5 and disappears at a draw ratio of 2.5, suggesting that strain-induced crystallization occurs during extension, which reduces the mobility of the PTT chain in the amorphous phase above a draw ratio of 2.5.

Figure 2a shows DSC scans of melt-crystallized PTT inside the DSC apparatus from 170 to 205 °C, while Figure 2b shows the DSC scans of melt-crystallized PTT from 110 to 160 °C in the melting region. Double- or triple-melting endotherms were observed for all PTT samples depending on the T_c. Triple-melting endotherms appear to be dominant at T_c below 195 °C, and double-melting endotherms are seen at T_c above 195 °C. These transitions are labeled as T_m^1, T_m^2, and T_m^3 (high-, middle-, and low-melting transitions, respectively). A similar behavior has been reported for a number of different semicrystalline polymers, and it is attributed to either melting of original and recrystallized crystals or crystals with multiple lamellar thicknesses. It can be clearly seen that T_m^2 merges with T_m^1 above $T_c = 190$ °C while T_m^3 increases in intensity relative to T_m^1 with increasing T_c above 170 °C. However, peak T_m^1 stays basically in the same position, but the intensity of T_m^1 decreases with increasing T_c. The DSC scan of melt-crystallized PTT at 210 °C has been reported recently[15] and has shown that there are two melting transitions. As the heating rate increased, the low-temperature transition increased in intensity whereas the high-melting transition decreased in intensity. Therefore, T_m^1

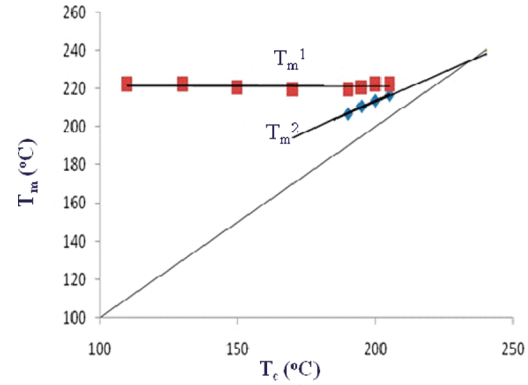

Figure 3. Melting transitions T_m^1 and T_m^3 versus T_c.

in our study is attributed to melting of secondary crystallites formed during recrystallization of primary crystallites, suggesting that the formation of recrystallized crystals by annealing PTT films melt crystallized above 170 °C is almost constant, even though the crystallinity of the initial sample is different. The secondary crystallites formed for the sample melt crystallized below 170 °C melt at lower temperature, indicating that these samples form less stable crystallites. Melting peak T_m^3 is attributed to the melting of primary crystallites that are formed during melt crystallization, and the thermal stability of these crystals is usually low. T_m^3 increases with increasing T_c, suggesting that the thermal stability of melt-crystallized PTT crystals increases with increasing T_c. It should be pointed out that T_m^3 is always about 10−15 °C higher than T_c.

Melting temperatures T_m^1 and T_m^3 are plotted against T_c in Figure 3. No significant change in T_m^1 was observed as a function of T_c, while T_m^3 strongly depends on T_c. T_m^3 was observed only for the samples melt crystallized above 170 °C, and it is always about 10 °C higher than T_c. It is apparent from Figure 3 that T_m^3 of PTT increases almost linearly with T_c. The equilibrium melting temperature (T_m^0) of PTT was determined by a Hoffman−Weeks plot using the extrapolation of a plot of T_m^3 versus T_c to $T_m^3 = T_c = 239$ °C, which is in very good agreement with the value of 238 °C previously reported by Pyda et al.[13] DSC heating scans of PTT melt crystallized at various T_c values from 110 to 205 °C inside the DSC before and after cooling to room temperature were compared; there was no apparent difference in the DSC scan before and after cooling to room temperature, and they are similar to the DSC scans of PTT melt crystallized in the oven.

Heat of fusion (ΔH) values of all melt-crystallized samples were obtained by taking the integrated area of the melting peak, and crystallinity values for PTT were determined by using the heat of fusion of 100% crystalline PTT. The heat of fusion of a perfect crystal was reported as 145.63 J/g.[13] Crystallinity values observed for melt-crystallized PTT inside the oven are plotted against T_c in Figure 4. It can be seen from Figure 4 that the crystallinity increases slowly up to $T_c = 190$ °C and increases rapidly when T_c exceeds 190 °C. Melt crystallization of PTT was carried out at 195 °C for 30 min and 1 h, and the crystallinities observed for both samples were approximately the same, suggesting that thermally induced crystallization quite strongly depends on the temperature but is less dependent on time. For example, the crystallinity of PTT melt crystallized for 30 min at 170 °C is 24%, compared to that of PTT crystallized for 1 h at 170 °C, which is 25%. Crystallinity values obtained for PTT films melt crystallized inside the DSC apparatus before and after cooling to room temperature are also shown in Figure 4. The samples after cooling to room temper-

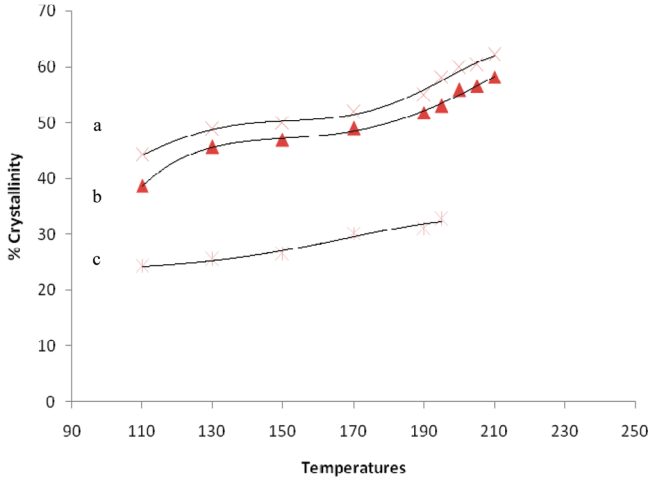

Figure 4. Crystallinity versus T_c obtained for PTT films melt crystallized inside the DSC apparatus after cooling to room temperature (a) and before cooling to room temperature (b) and inside the oven (c).

ature have extra crystallinity of about 3−4% compared to the samples before cooling to room temperature. The crystallinity differences between melt-crystallized PTT films before and after cooling to room temperature may be attributed to additional crystallinity developed during cooling by lamella thickening. Annealing of PTT was carried out inside the DSC apparatus,[28,29] and the difference in crystallinity observed before and after cooling the annealed PTT to room temperature was about 2%. It should be noted in Figure 4 that PTT crystallized in the oven provided a much lower crystallinity, suggesting fast quenching during crystallization of PTT in the oven compared to crystallization in the DSC apparatus may be responsible for the low crystallinity.

The crystallization kinetics of melt crystallization of PTT was determined by DSC by heating PTT samples to 260 °C, holding them at that temperature for 5 min to delete the prior thermal history, and cooling them to the desired T_c for 60 min. Crystallization exotherms vs the crystallization time of PTT melt crystallized at 150, 195, 200, and 205 °C were obtained, and the crystallization process took about 20−45 min depending on the T_c. The isothermal melt crystallization kinetics has been studied previously in detail using DSC above 200 °C,[15] and the kinetics of melt crystallization at low temperatures is investigated in the present study. The isothermal crystallization kinetics of PTT was analyzed using the double logarithm of the Avrami equation, $\ln[-\ln(1 - x(t))] = \ln(k) + n \ln(t)$, where $1 - x(t)$ is the weight fraction of amorphous material at time t, $x(t)$ stands for the weight fraction of crystallinity, n is the Avrami exponent which depends on the nucleation and growth of the polymer, k is the rate constant, and t is the time of crystallization. The value of n represents the crystallization mechanism and is determined from the slope, and k is determined from the intercept of the linear plot of $\ln[-\ln(1 - x(t))]$ vs $\ln(t)$. The values of n and k are listed in Table 1 along with the half-time of crystallization, $t_{1/2}$. $t_{1/2}$ is defined as the time required for the development of half of the final crystallinity. It is apparent from Table 1 that $t_{1/2}$ increases with increasing T_c as expected. Values of 2−3 were obtained, suggesting spherulitic morphology. Ideally, $n = 3$ indicates spherical growth and $n = 2$ suggests circular disk shape growth. A fractional number for n indicates heterogeneous nucleation. The determined n values suggest well-defined spherulitic morphology, which is consistent with our optical microscopic observations.

TABLE 1: Avrami Parameters and Half-Time of Crystallization for PTT Films Melt Crystallized Isothermally at Selected Temperatures

T_c (°C)	k	n	$t_{1/2}$ (min)
150	1.752	1.75	0.4
190	0.865	1.88	0.9
200	0.050	2.35	2.7
205	0.010	2.56	7.3

Figure 5 shows the optical micrographs of PTT melt crystallized at 110, 150, and 190 °C obtained by polarized light microscopy. Optical micrographs show spherulitic morphology, and it appears that the spherulite size depends on the crystallization temperature, which appears to be consistent with our kinetic data. A Maltese cross pattern is evident, indicating an orientation of the crystalline lamella along or perpendicular to the spherulitic radius. It can be seen that the spherulite size increases with increasing crystallization temperature, suggesting a slower crystallization rate at higher temperatures. The spherulitic size is apparently controlled by the kinetics of crystallization and amount of crystallinity. Sperulites observed here are nonbanded, which is consistent with the observation made in the previous study that banded spherulitic morphology has been observed only for the sample melt crystallized above 195 °C. The rate of crystallization is much slower at higher T_c, providing enough space between spherulites for them to grow larger. On the other hand, the nucleation density is much higher at low T_c due to faster crystallization that yielded smaller spherulites.

3.2. Conformational Characterization. It is well-known that infrared spectroscopy is a very powerful tool to study conformational and structural changes that take place on thermally induced and strain-induced crystallization. In the present study we utilize IR spectroscopy to determine conformational changes during melt crystallization of PTT. The infrared spectra collected in the region between 750 and 1650 cm^{-1} at room temperature for amorphous and melt-crystallized PTT at different T_c values are shown Figure 6. It appears there is an increase in the absorbance of bands at 933 (CH_2 rocking), 947 (CH_2 rocking), 1037 (C−C stretching), 1358 (CH_2 wagging), and 1465 (CH_2 bending) cm^{-1} and a decrease in absorbance of bands at 811, 976, and 1173 (CH in-plane bending of the aromatic ring), 1328 and 1385 (CH_2 wagging), 1452 (CH_2 bending), and 1577 cm^{-1} with increasing T_c. It was shown by DSC that melt crystallization of PTT films produces a significant amount of crystallinity which increases with increasing T_c. Therefore, the bands showing an increase in absorbance are attributed to the crystalline phase of PTT, while the bands showing a decrease in absorbance are associated with the amorphous phase of PTT. The band assignments for PTT have appeared in a number of papers,[26−31] and the band assignments were confirmed by us in our previous study.[29]

It has been reported that the trimethylene glycol unit ($-OCH_2CH_2CH_2O-$) of PTT adopts gauche and trans conformations through internal rotation through the C−C bond. In the crystalline phase, the $-OCH_2CH_2CH_2O-$ unit adopts the tggt conformation, whereas in the amorphous phase, $-OCH_2CH_2CH_2O-$ is mainly in the gttg conformation. The crystalline structure of PTT takes the tggt conformation because its energy is the lowest; the next higher energy conformation is gttg, and the all-trans tttt conformation is the highest energy conformation. The gttg conformation is the most populous in the amorphous phase of PTT.

Specific bands associated with gauche and trans conformations of the $-OCH_2CH_2CH_2O-$ unit appear in the region

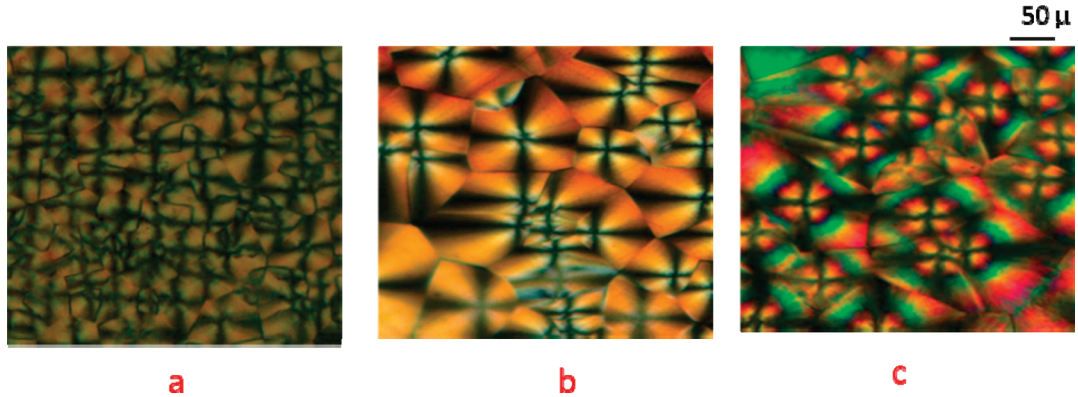

Figure 5. Optical micrograph of PTT isothermally melt crystallized at different temperatures: (a) 110 °C; (b) 150 °C; (c) 190 °C.

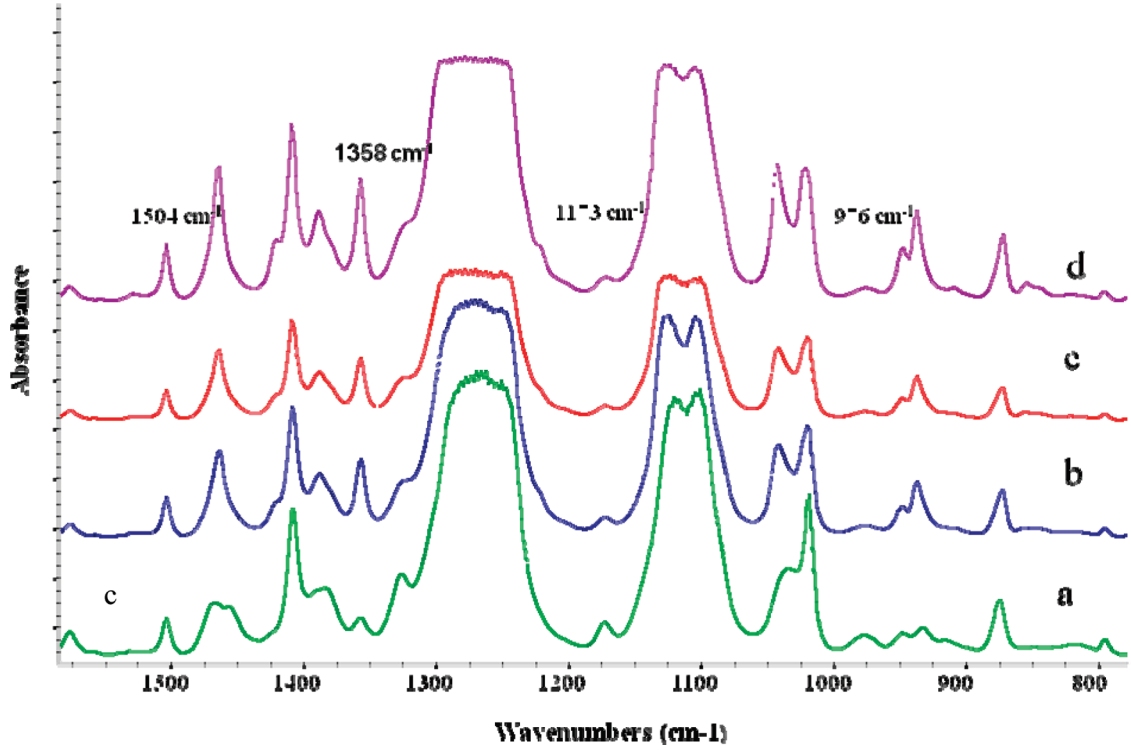

Figure 6. FTIR spectra for melted PTT at different ranges of temperatures in the region between 1600 and 780 cm^{-1}: amorphous (a), 110 °C (b), 150 °C (c), and 190 °C (d).

between 600 and 1500 cm^{-1}. The band at 1358 and 976 cm^{-1} associated with CH_2 wagging were attributed to the gauche (tggt) and trans (gttg) conformations of the glycol unit. It was demonstrated in our previous study that both crystalline and amorphous PTT spectra show a band at 1358 cm^{-1}, suggesting that the gauche conformation is present in both phases while the trans conformation is only present in the amorphous phase. A method has been developed in our laboratory to determine the amount of crystalline gauche, amorphous gauche, and amorphous trans conformations in PTT using the bands at 1358 and 976 cm^{-1}. The crystalline and amorphous gauche conformations of PTT during melt crystallization are determined using a combination of DSC and FTIR spectroscopy assuming a two-phase conformational model. The absorbances of bands at 1358 and 976 cm^{-1} were normalized to 1504 cm^{-1}, and the following expression can be written using the two-phase conformational model: $A_{1504}/A_{976} = P_1(A_{1358}/A_{976}) + P_2$, where P_1 and P_2 are constants associated with the gauche and trans conformations, respectively. The absorbance ratios were determined using the peak area tool. These experimental data were plotted to obtain constants P_1 and P_2. P_1 and P_2 were determined by A_{1504}/A_{976} vs A_{1358}/A_{976} as 0.23 and 4.9, respectively. The fractions of gauche and trans conformations present in PTT melt crystallized at various T_c values were determined by $P_1(A_{1358}/A_{1504})$ and $P_2(A_{976}/A_{1504})$, respectively. It is worth mentioning again that $P_1(A_{1358}/A_{1504})$ consists of amorphous gauche and crystalline gauche conformations.

Trans and gauche conformations estimated by this method are compared with the crystalline fraction obtained by DSC in Table 2. The DSC crystallinity is always lower than the percentage of gauche conformers, confirming that the gauche conformation is present not only in the crystalline phase but also in the amorphous phase. The crystalline gauche and amorphous gauche conformations were separated by combining the DSC crystallinity and total gauche conformation, given in Table 2. The crystalline gauche conformation is equal to the fraction of crystalline phase obtained using DSC, and the amorphous gauche conformation then can be obtained by subtracting the crystalline gauche conformation from the total gauche conformation, also given in Table 2. The fractions of crystalline gauche, amorphous gauche, and trans conformations are plotted against the crystallization temperature in Figure 7.

TABLE 2: Fractions of Crystalline Gauche, Amorphous Gauche, and Trans Conformations as a Function of the Crystallization Temperature[a]

T_c	crystallinity (%)	$P_1(A_{1358}/A_{1504})$ (crystalline gauche)	$1 - P_1(A_{1358}/A_{1504})$ (trans)	amorphous gauche
110	0.24	0.30	0.71	0.06
130	0.25	0.32	0.68	0.07
150	0.26	0.34	0.67	0.08
170	0.30	0.37	0.66	0.07
190	0.31	0.40	0.60	0.09
195	0.33	0.43	0.52	0.09

[a] All of the data points are averages of at least three determinations. The standard deviation is ±0.02.

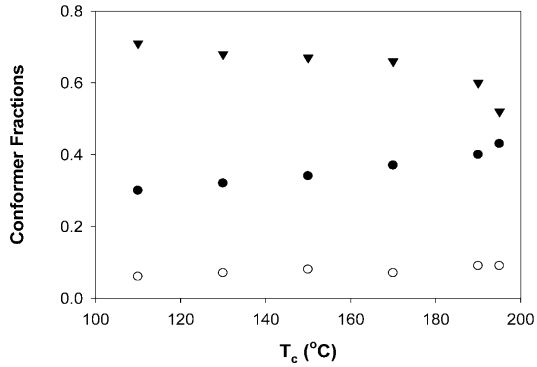

Figure 7. Fractions of the amorphous gauche (○), crystalline gauche (●), and trans (▲) conformers against the melt T_c. The data points are the means of at least three determinations. The standard deviation is ±0.02.

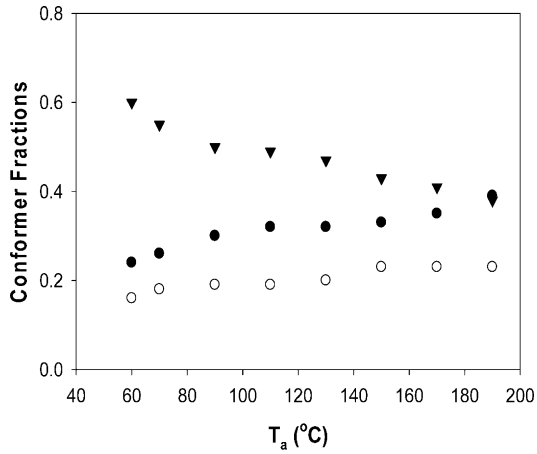

Figure 8. Fraction of the amorphous gauche (○), crystalline gauche (●), and trans (▲) conformers against T_a. The data points are the means of at least three determinations. The standard deviation is ±0.02.

It can be seen from the figure that the amorphous gauche conformation increases slightly with increasing crystallization temperature (from 6% to 10%). The increase in the amorphous gauche conformation is not significant compared to the increase in the crystalline gauche conformation with increasing T_c.

The conformational changes during annealing of PTT were investigated and showed a significant increase in the crystalline and amorphous gauche conformations with increasing annealing temperature, T_a. Figure 8 reproduces the conformational changes as a function T_a for comparison. It appears the fraction of the trans conformation decreases while the fraction of the crystalline gauche conformation increases as a function of T_a. The amorphous gauche conformation also increases up to $T_a = 160$ °C and then stays constant at $T_a > 160$ °C. This observation indicates that the mechanisms associated with crystallization during annealing and melt crystallization are different. Conformational changes during thermally induced and strain-induced crystallization of PET have been studied extensively, and it has been reported that amorphous PET consists of trans and gauche conformations whereas crystalline PET contains only the trans conformation and the amorphous trans conformation transforms into the crystalline trans conformation during the initial stage of the crystallization. Conformational changes during thermally induced crystallization of PTT are different from those of PET, and the amorphous gauche and crystalline gauche conformations in PTT increase with T_c. The extent of the increase strongly depends on the type of crystallization, whether it is annealing or melt crystallization.

Conclusions

The melt crystallization of PTT was studied using differential scanning calorimetry, optical microscopy, and FTIR spectroscopy. Double- or triple-melting endotherms were observed for all PTT samples depending on T_c. High-, middle-, and low-melting endotherms were labeled as T_m^1, T_m^2, and T_m^3, respectively. T_m^2 disappears above $T_c = 190$ °C, while T_m^3 increases in intensity with increasing T_c above 170 °C. However, the peak T_m^1 stays basically in the same position, but the intensity of T_m^1 decreases with increasing T_c. Therefore, T_m^1 was attributed to melting of secondary crystallites formed during recrystallization of primary crystallites. T_m^3 was always about 10 °C higher than T_c. T_m^0 of PTT was determined by a Hoffman−Weeks plot using an extrapolation of a plot of T_m^3 versus T_c to $T_m^3 = T_c = 239$ °C, which is in very good agreement with the reported value of 238 °C. Crystallinity values increased with increasing T_c for both melt-crystallized PTT inside the DSC apparatus and inside the oven. Additional crystallinity of about 3−4% developed during cooling was attributed to lamella thickening. The crystallization kinetics were analyzed using the Avrami equation. The value of 2−3 obtained for the Avrami constant n suggested that PTT crystallized in two-dimensional to three-dimensional morphology. Bands at 1358 and 976 cm^{-1} were used to determine the trans and gauche conformations of methylene segments. Combining the total gauche conformation with the DSC crystallinity, the crystalline and amorphous gauche conformations were separated. It was found that the crystalline gauche conformation increases and the amorphous trans conformation decreases with increasing T_c while the amorphous gauche conformation showed no significant change with increasing T_c.

References and Notes

(1) Ward, I. M.; Wilding, M. A.; Brody, H. J. *J. Polym. Sci., Polym. Phys.* **1976**, *14*, 263.
(2) Brown, H. S.; Chuah, H. H. *Chem. Fibers Int.* **1997**, *47*, 72.
(3) Lee, H. S.; Park, S. C.; Kim, Y. H. *Macromolecules* **2000**, *33*, 7994.
(4) Wu, G.; Li, H. W.; Wu, Y. Q.; Cuculo, J. A. *Polymer* **2002**, *43*, 4915.
(5) Chang, J. H.; Kim, S. J.; Im, S. *Polymer* **2004**, *45*, 5171.
(6) Luo, W.; Liao, Z.; Yan, J.; Li, Y.; Chen, X.; Mai, K.; Zhang, M. *Macromolecules* **2008**, *41*, 7513.
(7) Chuah, H. H. *J. Polym Sci., Polym. Phys.* **2002**, *40*, 1513.
(8) Goodman, I. *Angew. Chem.* **1962**, *74*, 606.
(9) Traub, H. L. *Angew. Makromol. Chem.* **1995**, *179*, 4055.
(10) Gonzalez, C. C.; Perena, J. M.; Bello, A. *J. Polym. Sci., Polym. Phys.* **1988**, *26*, 1397.
(11) Cheng, S. Z. D.; Wunderlich, B. *Macromolecules* **1988**, *21*, 789.
(12) Chuah, H. H. *J. Polym. Sci., Polym. Phys.* **2002**, *40*, 1513.
(13) Pyda, M.; Boller, A.; Grebowicz, J.; Chuah, H.; Lebedev, B. V.; Wunderlich, B. *J. Polym. Sci., Polym. Phys.* **1998**, *36*, 2499.
(14) Chuah, H. H. *Polym. Eng. Sci.* **2001**, *41*, 308.

(15) Huang, J. M.; Chang, F. C. *J. Polym. Sci., Polym. Phys.* **2000**, *38*, 934.
(16) Desborough, I. J.; Hall, I. H.; Neisser, J. Z. *Polymer* **1979**, *20*, 545.
(17) Poulin-Dandurand, S.; Perez, S.; Revol, J. F.; Brisse, F. *Polymer* **1979**, *20*, 419.
(18) Jakeways, R.; Ward, I. M.; Wilding, M. A.; Desborough, I. J.; Pass, M. G. *J. Polym. Sci., Polym. Phys.* **1975**, *13*, 263.
(19) Chuah, H. H. *Macromolecules* **2001**, *34*, 6985.
(20) Shafee, E. E. *Polymer* **2003**, *44*, 3727.
(21) Ward, I. M.; Wilding, M. A. *Polymer* **1977**, *18*, 327.
(22) Lin, S. B.; Koenig, J. L. *J. Polym. Sci., Polym. Phys.* **1982**, *20*, 2277.
(23) Rodriquez-Cabello, J. C.; Santos, J.; Merino, J. C.; Pastor, J. M. *J. Polym. Sci., Polym. Phys.* **1996**, *34*, 1243.
(24) Ouchi, I.; Hosoi, M.; Shimotsuma, S. *J. Appl. Polym. Sci.* **1977**, *21*, 3445.
(25) Tzou, D. L.; Huang, T. H.; Desai, P.; Abhiraman, A. S. *J. Polym. Sci., Polym. Phys.* **1993**, *31*, 1005.
(26) Kim, K. J.; Bae, J. H.; Kim, Y. H. *Polymer* **2001**, *42*, 1023.
(27) Bulkin, B. J.; Lewin, M.; Kim, J. *Macromolecules* **1987**, *20*, 830.
(28) Vasanthan, N.; Yaman, M. *J. Polym. Sci., Polym. Phys.* **2007**, *45*, 1675.
(29) Yaman, M.; Ozkaya, S.; Vasanthan, N. *J. Polym. Sci., Polym. Phys.* **2008**, *46*, 1497.
(30) Park, S. C.; Liang, Y.; Lee, H. S. *Macromolecules* **2004**, *37*, 5607.
(31) Ouchi, I.; Hosoi, M.; Shimotsuma, S. *J. Appl. Polym. Sci.* **1977**, *21*, 3445.

JP1058484